Quantification of material nonlinearity in relation to microdamage density using nonlinear reverberation spectroscopy: Experimental and theoretical study

K. Van Den Abeele[a)]
Interdisciplinary Research Center, K.U. Leuven Campus Kortrijk, Etienne Sabbelaan 53, B-8500 Kortrijk, Belgium

P. Y. Le Bas
Interdisciplinary Research Center, K.U. Leuven Campus Kortrijk, Etienne Sabbelaan 53, B-8500 Kortrijk, Belgium and Los Alamos National Laboratory, EES-17, MS-D443, Los Alamos, New Mexico 87544

B. Van Damme
Interdisciplinary Research Center, K.U. Leuven Campus Kortrijk, Etienne Sabbelaan 53, B-8500 Kortrijk, Belgium

Tomasz Katkowski
Interdisciplinary Research Center, K.U. Leuven Campus Kortrijk, Etienne Sabbelaan 53, B-8500 Kortrijk, Belgium and Institute of Experimental Physics, University of Gdansk, Ulica Wita Stwosza 57, 80-952 Gdańsk, Poland

(Received 28 October 2008; revised 29 June 2009; accepted 30 June 2009)

High amplitude vibrations induce amplitude dependence of the characteristic resonance parameters (i.e., resonance frequency and damping factor) in materials with microscopic damage features as a result of the nonlinear constitutive relation at the damage location. This paper displays and quantifies results of the nonlinear resonance technique, both in time (signal reverberation) and in frequency (sweep) domains, as a function of sample crack density. The reverberation spectroscopy technique is applied to carbon fiber reinforced plastic (CFRP) composites exposed to increasing thermal loading. Considerable gain in sensitivity and consistent interpretation of the results for nonlinear signatures in comparison with the linear characteristics are obtained. The amount of induced damage is quantified by analyzing light optical microscopy images of several cross-sections of the CFRP samples using histogram equalization and grayscale thresholding. The obtained measure of crack density is compared to the global macroscopic nonlinearity of the sample and explicitly confirms that the increase in nonlinearity is linked to an increased network of cracks. A change from 1% to 3% in crack density corresponds to a tenfold increase in the signature of nonlinearity. Numerical simulations based on a uniform distribution of a hysteretic nonlinear constitutive relation within the sample support the results.
 [DOI: 10.1121/1.3184583]

PACS number(s): 43.25.Dc, 43.25.Ba, 43.25.Gf, 43.25.Zx [ROC] Pages: 963–972

I. INTRODUCTION

Safety and reliability of large and small scale engineering structures are of crucial importance. In aeronautics, for instance, the performance and behavior characteristics of airframe structures can be adversely affected by structural degradation resulting from sustained use within normal flight envelopes, as well as from exposure to severe environmental conditions or from damage due to unexpected impacts. The timely and accurate detection, characterization, and monitoring of the development of structural defects over time (e.g., cracking, corrosion, delamination, and material degradation) are a major concern in the operational environment. If the authors are to improve the accuracy of structural integrity predictions, they must minimize the uncertainty associated with critical parameters for early degradation, incipient damage, and progressive failure modes in components. Hence, huge efforts are devoted to the development of enhanced, reliable, and integrated measurement systems and protocols for identifying microcracks in structural engineering components. As part of this effort, researchers all over the world are currently developing and validating innovative microdamage inspection system based on various nondestructive testing methods within the class of nonlinear elastic wave spectroscopy (NEWS).[1,2]

NEWS techniques primarily deal with the investigation of the amplitude dependence of material parameters such as wave speed, attenuation, and spectral content. The degree to which these material properties depend on the applied dynamic amplitude can be quantified by various nonlinearity parameters. Several NEWS techniques have been developed to probe for the existence of damage (e.g., delaminations, microcracks, and weak adhesive bonds) by investigating the

[a)]Author to whom correspondence should be addressed. Electronic mail: koen.vandenabeele@kuleuven-kortrijk.be

generation of harmonics and intermodulation of frequency components,[3–11] the amplitude-dependent shift in resonance frequencies,[11–15] the nonlinear contribution to attenuation properties,[15] slow dynamic effects,[15–18] and phase modulation.[19] Laboratory tests performed on a wide variety of materials subjected to different microdamage mechanisms of mechanical, chemical, and thermal origins have shown that the sensitivity of such nonlinear methods to the detection of microscale features is far greater than that obtained with linear acoustical methods.[6,8,13,20–23]

In this paper, the authors restrict themselves to a new variation of the nonlinear resonance technique. Single mode nonlinear resonant ultrasound spectroscopy (SIMONRUS)[12,13] is a well-known frequency domain method analyzing resonance sweeps at increasing excitation amplitude; the authors here introduce its time domain variant, which analyzes the instantaneous changes in the resonance characteristics during the reverberation of an object after being excited near resonance. This technique, called nonlinear reverberation spectroscopy (NRS), is an improved version of an earlier reported time domain resonance technique (time domain SIMONRUS) that has been used to analyze mechanical fatigue in titanium and concrete.[22,24] The main advantage over SIMONRUS is that the discrete frequency sweep for several amplitudes of excitation is replaced in NRS by a simple time signal recording at a single excitation level. Hence, NRS is significantly faster and requires fewer acquisitions. After presenting the general ideas behind NRS in Sec. II, the authors apply the new version to composite laminates [carbon fiber reinforced plastics (CFRPs)] with various degrees of thermal loading, simulating the initiation of global microdamage as the result of extreme environmental conditions (Sec. III). These results will be put side by side with a measure of the crack density of the samples via image analysis in the third part. To the authors' knowledge, this is the first real experimental quantification of nonlinearity in terms of crack density. In the Conclusion (Sec. VI), the authors present a theoretical model of a resonating flexural beam including nonlinear mechanical properties to explain the observed nonlinear behavior.

II. NRS

Nonlinear resonance spectroscopy techniques investigate the resonance behavior of objects under amplitude-dependent response. Generally, a single resonance mode of the object with associated resonance frequency is selected. In SIMONRUS,[12,13] the object is subjected to a frequency sweep around this resonance frequency at constant excitation amplitude. The true resonance characteristics, frequency and damping factor (or quality factor), are then analyzed from fits of the resulting frequency response amplitude (resonance curve). This is repeated for increasing levels of excitation amplitudes. By plotting the resonance characteristics at each level versus the maximum response amplitude at the same level, one can analyze the amplitude dependence or nonlinearity of the object. Intact materials show no change in the resonance characteristics, whereas damaged materials generally show a decrease in the resonance frequency with amplitude (nonlinear softening) and an increase in the damping factor ($1/Q$, with Q as the quality factor) due to nonlinear attenuation.[15,22,24]

NRS is the time domain analogy of SIMONRUS. In NRS, a sample is excited at constant excitation amplitude and constant frequency for a certain period of time. The frequency is chosen in the neighborhood of one of the resonance frequencies of the sample. After a number of cycles, sufficient for the sample to reach its steady state response, the continuous wave excitation is stopped, say, at $t=t_0$, and the reverberation response of the sample is measured from t_0 to t_1 and stored for analysis. The reverberation signal is typically a decaying time signal, with large amplitudes near t_0 and smaller amplitudes near t_1. Appropriate synchronization allows averaging of the signal, and a feedback loop can be used to optimize the dynamic range as function of the measurement time. Several sections recorded at decreasing dynamic range are finally selected and matched to create a composed signal with adequate vertical resolution. The decay signal is then analyzed using a successive fitting of an exponentially decaying sine function,

$$A_k e^{-\alpha_k t} \sin(2\pi f_k t + \phi_k), \tag{1}$$

to small time windows (approximately 20 cycles). Here, A_k denotes the amplitude, α_k is the decay parameter, f_k is the frequency, and ϕ_k is the phase of the signal in the kth window. This allows the creation of a parametric plot of the true resonance frequency f_k and of the decay parameter α_k as function of the amplitude A_k, thereby providing information on the occurrence of nonlinearity. If the material is linear, the frequency in different windows of the reverberation signal remains constant. If the material is nonlinear, the frequency in the reverberation signal gradually increases with decreasing amplitude and thus with time, in agreement with the nonlinear softening effect on the modulus due to the presence of nonlinearity.[25,26]

In practice, depending on the sample (size and weight) and the resonance frequency of the mode, both experiments, SIMONRUS and NRS, can be performed in a fully noncontact mode by means of a loudspeaker as exciter and a laser Doppler vibrometer for the response measurement. The schematic setup and a typical NRS response and analysis of the data for one of the samples considered in Sec. III (thermal shocked CFRP) can be found in Fig. 1. The amplitude dependence of resonance frequency and damping are clear markers of the nonlinear material behavior. When the amplitudes are recalculated in terms of strain (see later), a NRS nonlinearity parameter can be deduced from the proportionality relation as the slope of the relative change.

Figure 2 shows the consistency between the two resonance methods. The analyzed resonance frequency from the frequency sweeps shows the same slope (nonlinearity) as the analyzed resonance frequency deduced from the reverberation signal. There is a small offset related to the change in experimental conditions. The advantage of the NRS method is that it requires fewer acquisitions (one time signal at a single excitation level versus a discrete frequency sweep at

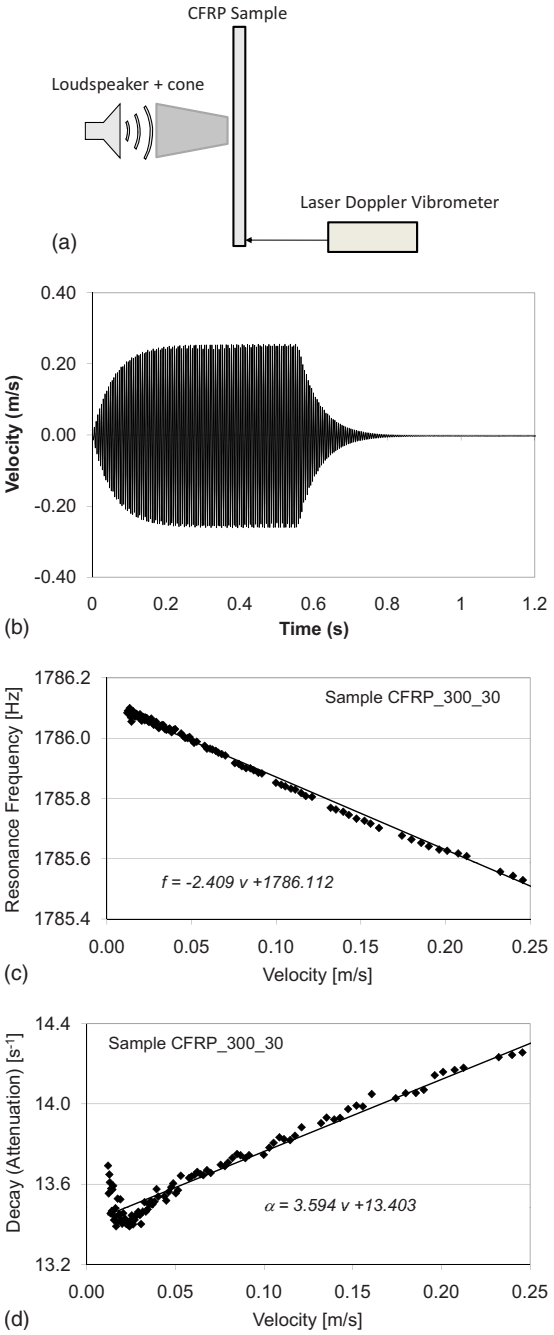

FIG. 1. (Color online) The NRS method and its typical results. (a) NRS experimental setup: The sample is excited by a loudspeaker, and the particle velocity is recorded by means of a laser Doppler vibrometer. (b) Full recorded signal. (c) Analysis of the instantaneous resonance frequency versus particle velocity amplitude for a CFRP sample shocked at 300 °C for 30 min. (d) Analysis of the instantaneous damping characteristic versus particle velocity amplitude for the same sample.

various increasing levels of excitation) and, by such, that it is faster than SIMONRUS even if more post-acquisition data analysis is needed.

The robustness of the method has been tested in several ways. Being a non-contact experiment, the only concern that could affect reproducibility is the string support of the sample. Paying particular attention to put the supporting strings near the nodes, several experiments were repeated after dismounting and remounting without major deviations in the results (errors of a few percent). In addition, even

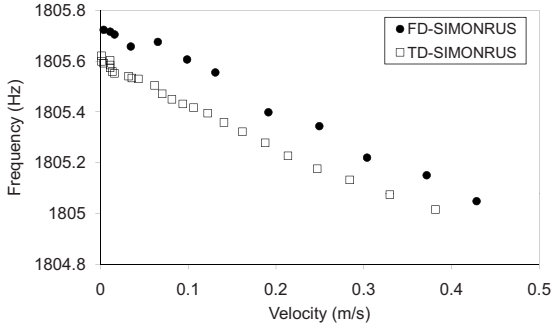

FIG. 2. Illustration of the consistency between the SIMONRUS and NRS results (sample CFRP_300_60).

though experimental conditions may significantly affect the resonance frequency, the slope of the amplitude dependence, which yields the measure of the nonlinearity parameter in the NRS experiment, is independent of the exact resonance frequency value as it merely depends on the relative changes of it with respect to amplitude. These relative changes seem to be less dependent on the experimental conditions than the values of the resonance frequency. On top of this, the authors also verified that the obtained slope in the proportionality relations is independent of the chosen initial excitation frequency and applied voltage. The results of these investigations are illustrated in Fig. 3. In Fig. 3(a), the analyzed response at three different frequencies in the neighborhood of the resonance frequency is illustrated for a fixed excitation amplitude. In Fig. 3(b), the response at a fixed excitation frequency is illustrated for three different excitation amplitudes. The conclusion is that the NRS nonlinearity parameter is independent of the initial excitation frequency (within limits in the order of the full width at half maximum of the resonance curve) and applied voltage (for regimes that do not involve slow dynamics). Together with the high sensitivity of the NRS nonlinearity parameter to damage (see Sec. III), this relative insensitivity to changes in the experimental setup and conditions, in comparison to linear resonance measurements, is of primary and practical advantage for the method.

III. APPLICATION TO THERMALLY LOADED CFRP

In this section, the authors illustrate the potential of the NRS techniques to discern heat damage in CFRPs and to validate its postulated high sensitivity to early damage and micromechanical changes in the medium.

A. CFRP and heat damage

CFRP is commonly used in the aircraft construction industry. It is expected that the next generation of airplanes will consist of more than 60% of composite structures.[27] Even though composite materials hold important advantages over aluminum, CFRP is also prone to various degradation mechanisms. The exposure to heat, for instance, induces chemical and microstructural changes affecting the mechanical behavior of the composite laminate, even at moderate temperatures.[28] Traditional nondestructive quality control techniques are often limited in their capabilities to detect and characterize subtle changes in the material properties associ-

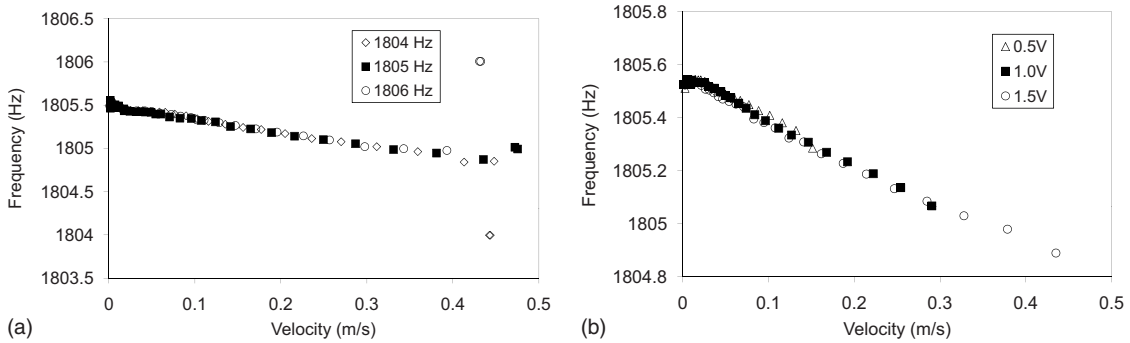

FIG. 3. Verification of the reliability of the NRS results for a single sample (CFRP_300_60) at various excitation frequencies (1804, 1805, and 1806 Hz) for fixed amplitude (1 V) (left) and at various excitation amplitudes (0.5, 1, and 1.5 V) for fixed excitation frequency (1805 Hz) (right).

ated with heat damage. A review of the mechanisms of heat damage in composites and a state-of-the-art of nondestructive evaluation (NDE) techniques currently used to evaluate heat damage is available in Refs. 28 and 29. Studies have shown that thermal degradation is typically matrix dominated since by the time fiber properties such as tensile strength and modulus are affected, all other mechanical integrity is lost. Mechanical metrics such as compressive, shear, and flexural strength and stiffness properties are believed to be the most sensitive properties for use in the early detection of thermal degradation, as opposed to nonmechanical parameters such as thermal and dielectric properties. Most of the work reported in the literature dealing with NDE for heat damage in composites is based on the following five methods: thermal (IR), ultrasonics, acoustic emission, dielectric properties, and radiography. These methods, while being readily available and generally well developed, are limited in their capabilities to detect and characterize the changes in composite material properties associated with heat damage. For instance, the detectability threshold of heat damage (1 h exposure at temperatures 200–300 °C) in unidirectional AS4-8552 CFRP laminates using conventional ultrasonics (immersed transmission C-scan imaging) was found at 290 °C.[30] Nevertheless, the measured value of the interlaminar shear strength for the same type of samples changed from 121 MPa for nonexposed samples to 114 MPa when exposed at 200 °C, to 84 MPa for 285 °C, and to 43 MPa for samples exposed at 300 °C for the duration of 1 h.

Most traditional NDE techniques are capable of detecting physical anomalies such as cracks and delaminations. However, to be effective for thermal degradation, they must be capable of detecting initial heat damage, which occurs at a microscopic scale. Review of the literature from more recent years indicates that a vast number of NDE methods are currently under development and show various degrees of promise for characterizing heat damage in composites. More extensive information on the status of development of several of these NDE methods and their capabilities for detecting heat damage in composite laminates can be found in an extended state-of-the-art review available from NTIAC.[29]

B. The NRS results

The authors examined a set of heat damaged composite laminate samples using the above described NRS technique and quantified their NRS nonlinearity parameters as function of the heating temperature and exposure time. The set of 21 CFRP (AS4/8552 quasi-isotropic lay-up) samples consisted of one reference sample, which was left unexposed, and 20 samples exposed at five different temperatures (240, 250, 260, 270, and 300 °C) for four different durations (15, 30, 45, and 60 min). The samples were cooled under ambient conditions and tested at room temperature. The nominal size of the samples was 120 mm (L) $\times$ 20 mm (W) $\times$ 4 mm (T). It is expected that thermal damage is induced in a more or less uniform manner over the sample volume.

The resonance mode under consideration in this study is the fundamental flexural mode of a beam, which has a stress concentration in the middle of the sample and displacement nodes at a distance of $0.224L$ from both edges, with L as the length of the sample (120 mm).[31,32] In the experimental setup, the sample is supported by two nylon wires at the node lines and is excited at a pure tone by a loudspeaker (diameter of 32 mm, the sound being concentrated by a converging cone of 180 mm length and 20 mm exit diameter) centered in the middle of the sample. The response is measured by a laser vibrometer (Polytec OFV303, decoder VD02) near one of the edges. All equipment is computer controlled and operated through LABVIEW and GPIB. The acquisition of the signal is realized by a 5 MHz DAQ-card.

In the NRS experiment, the authors excited the sample with a 1000 period burst excitation at a given amplitude and with a frequency close to the fundamental flexural resonance frequency. They then recorded a total of 0.6 s (120 000 points at a sampling rate of 200 kHz) of the reverberation of the sample after the excitation was stopped. Figure 1(b) shows a typical response from the start of the excitation to the steady state and the reverberation. To achieve a high accuracy in the recording of the reverberation signal, the authors implemented a variable dynamic range acquisition procedure based on an automated feedback of the instantaneous amplitude response. In this procedure, the dynamic range is decreased successively. At each range, signals are acquired and averaged ten times. The various signals recorded at decreasing dynamic range are finally matched to create a composed signal with adequate vertical resolution over the entire time axis.

The amplitude, frequency, and damping information contained in the resulting signal are then analyzed by divid-

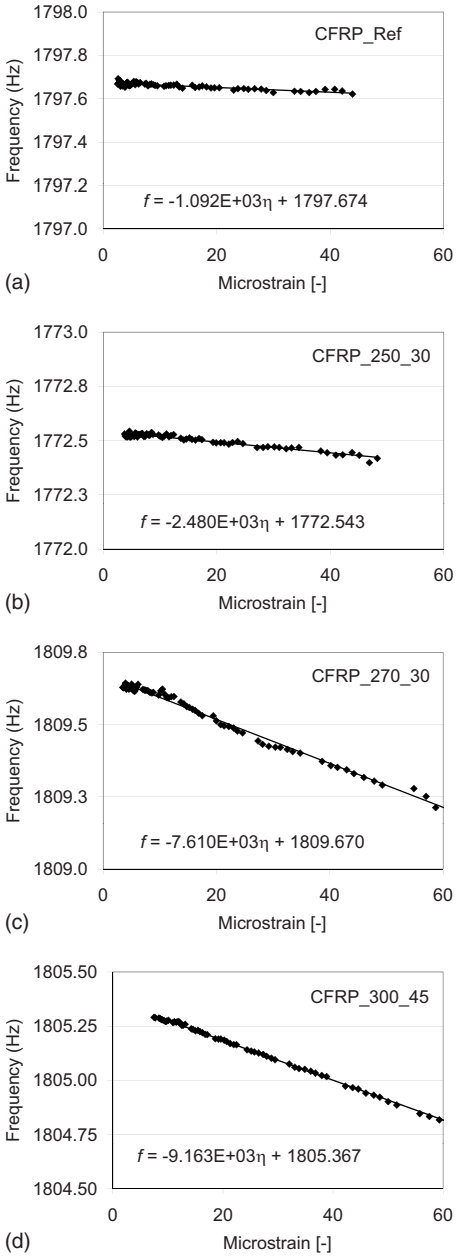

FIG. 4. NRS results showing the analyzed frequency versus microstrain amplitude for the reference sample showing almost no nonlinearity and for three samples at different heating temperatures and exposure times: 250 °C for 30 min, 270 °C for 30 min, and 300 °C for 45 min.

ing the composed signal into several windows (with fixed time duration of 10 ms, which is typically of the order of 20 periodic oscillations) and by fitting the previously described exponentially decaying sine function [Eq. (1)] to the data using a Levenberg–Marquardt algorithm to determine the parameters f_k, α_k, ϕ_k, and A_k, with k referring to the kth time window. This yields the evolution of the frequency (f_k) and damping characteristic (α_k) as function of the amplitude A_k in the decaying signal. Figure 4 shows the results for the instantaneous resonance frequency versus amplitude for the reference sample, for two samples exposed for 30 min at 250 and 270 °C, respectively, and for a sample heated at 300 °C for 45 min. The analyzed data for the reference sample nearly follow a horizontal line, meaning that there is no or minimal dependence of the frequency on the amplitude. The reference sample is thus close to being a linear material. On the other hand, the results for longer exposure and higher temperature show an increased frequency dependence on amplitude, which indicates an increase in the material nonlinearity. Changing the window size for the analysis of the reverberating signal (within limits, of course) did not influence the results.

In order to quantify the degree of nonlinearity, the authors calculated the NRS nonlinearity parameter Γ as the proportionality coefficient between the relative resonance frequency shift and the strain amplitude η,

$$\frac{\Delta f}{f_0} = \Gamma \eta, \tag{2}$$

with f_0 as the linear resonance frequency and $\Delta f = f_0 - f$. The strain amplitude values, η, were calculated from the measured particle velocity amplitude values, v, using the strain-velocity conversion expression for beams,[31,32]

$$\eta \approx 0.219 \frac{T}{f\sqrt{12}} \left(\frac{4.73}{L}\right)^2 v, \tag{3}$$

with $T=4$ mm and $L=120$ mm. It should be noted that because of the global character of the applied NEWS method, Γ only represents a global quantification of the nonlinearity, integrated over the whole sample. It contains no direct information on the localization of the defects. The values for the global NRS nonlinearity parameter Γ obtained in this study range from 0.6 to 10, and its variation as function of temperature and exposure time for all samples is summarized in Fig. 5(a). The authors observed an overall increase with increasing exposure time and heat temperature up to a factor of 10 with respect to the reference value. The obtained values are comparable to values obtained for intact samples of heterogeneous materials such as slate (30),[13] pultruded composites (5–10),[21] concrete (45),[22] and other materials (rocks and metals).[14,15]

A similar behavior can be observed when analyzing the nonlinearity in the damping characteristic,

$$\frac{\Delta \alpha}{\alpha_0} = \Upsilon \eta, \tag{4}$$

with α_0 as the linear time constant (connected to the attenuation). However, the errors in the analysis results are larger (support of the samples is very critical for attenuation), and the fits are not as clean as the ones dealing with the resonance frequency shift, which results in a less pronounced evolution [Fig. 5(b)].

C. Comparison with the linear resonance results and discussion

The NRS analysis also provides the linear resonance signatures such as linear attenuation and linear resonance frequency. Ignoring subtle geometry changes, it is possible to calculate the global stiffness (Young's modulus E_0) for the different samples from the linear resonance frequency values. However, the authors could not observe a systematic change as function of the temperature and exposure time

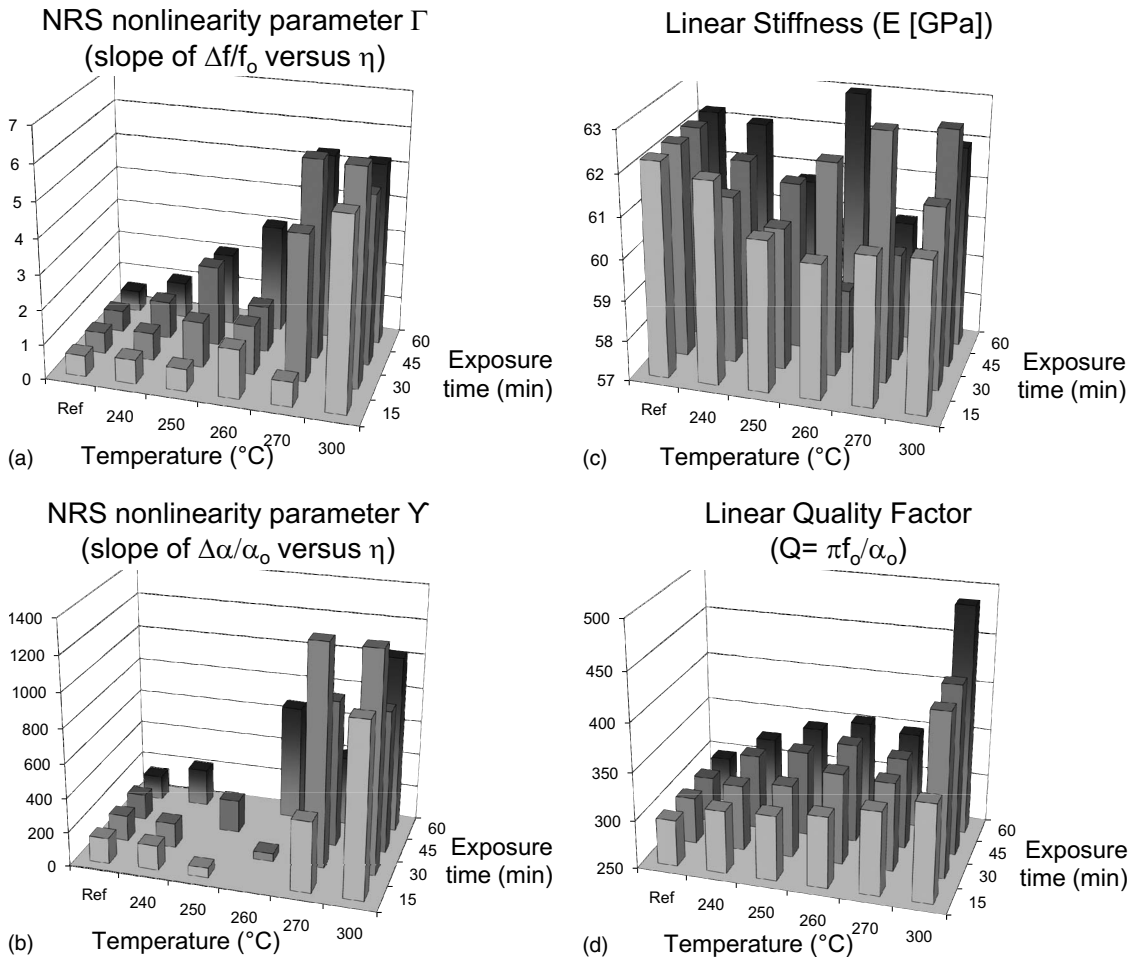

FIG. 5. Summary of the NRS results for all 21 samples as function of heating temperature and exposure time: (a) NRS nonlinearity parameter Γ deduced from the frequency response, (b) NRS nonlinearity parameter Γ deduced from the damping response (some Γ-values with low repeatability are omitted), (c) linear values of the stiffness E, and (d) linear Q-factor (inverse attenuation). The reference point was duplicated for different exposure times to help visualize the trend of the evolution of the parameters with temperature.

[Fig. 5(c)]. For the attenuation, on the other hand, they found that the linear value of the quality factor Q_0 (inverse attenuation $Q_0 = \pi f_0 / \alpha_0$) increases with temperature and exposure time [Fig. 5(d)], meaning that the attenuation (at that frequency) decreases with increasing damage. This is somewhat counterintuitive as one expects attenuation to increase with damage.

Without pretending that the authors are experts in this field, they conjecture that the decrease in the linear attenuation is associated with the chemical alteration in the matrix connected to fluids and fluid expulsion upon thermal loading. The reduction in fluids and the chemical adaptation processes generally lead to a decrease in attenuation, which in this case might dominate the expected increase in attenuation due to the formation of microcracks. In any case, it is obvious from this analysis that the nonlinear parameters derived in the NRS method show a considerable gain in sensitivity and provide a consistent interpretation of the results in contrast with the linear characteristics.

IV. QUANTIFICATION OF THE NRS NONLINEARITY PARAMETER IN RELATION TO THE MICROCRACK DENSITY

It is generally accepted that the dislocation buildup and the presence of cracks in damaged samples result in a macroscopically observed nonlinear behavior: The higher the crack density, the more pronounced the nonlinear signature of the sample will be. To check this idea and to quantify the obtained values of NRS nonlinearity parameter Γ with respect to the microcrack density, the authors sliced five of their samples in the thickness direction and extracted the crack density from each sample at the surface. The samples are first imaged using light optical microscopy (LOM) coupled to a digital camera. Images are acquired with the magnification level set to 2. For each sample, the entire surface of the transversal and longitudinal cuts is captured sequentially by imaging small size rectangles covering the entire surface. The images are then combined to generate a full picture. Two such raw images are shown in Fig. 6.

The process to quantify the crack density is performed on subsets of the entire image, the size of which is determined by the processing speed of the computer used to perform the image treatment. The "crack density" analysis for each subset consists of six standard steps:

1. selection of the zones such that only the areas with fibers oriented out of plane are analyzed,
2. edge detection using Sobel's technique[33] and conversion in grayscale,
3. equalization of the image,[34]

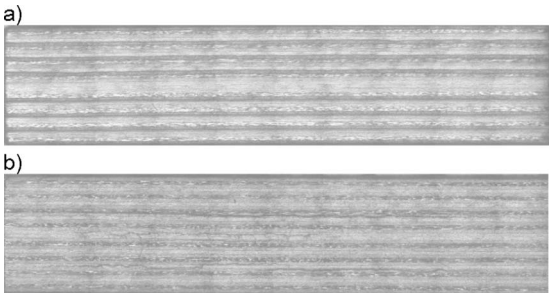

FIG. 6. Original images of CFRP layers (composed of overlapping digital shots using a LOM). (a) Transversal cut for the reference sample. (b) Transversal cut for the sample treated at 270 °C for 60 min.

4. thresholding to get binary images,
5. elimination of isolated points, and
6. determination of the crack density as the ratio of the black pixels to the total number of pixels after the final stage in the image treatment.

When performing a similar treatment for all subsets of the original image, the authors obtained Fig. 7, which compares the original raw image to the binary end result. The figure also contains a more detailed view, obtained with a scanning electron microscope, of a typical thermally induced crack in the region of the tip and in the central region.

The results of this treatment applied to all images leads to Fig. 8. Open diamonds represent the different values of the crack density obtained in several subsets of the images. The spread of the results is mainly due to the small size of the subset area, which is analyzed and illustrates the statistical variation as function of the position along the surface. As one can expect, some areas show almost no cracks, while others exhibit several. The filled circles are the average value for each sample. The authors observed a clear relationship between the NRS nonlinearity parameter Γ and the crack density.

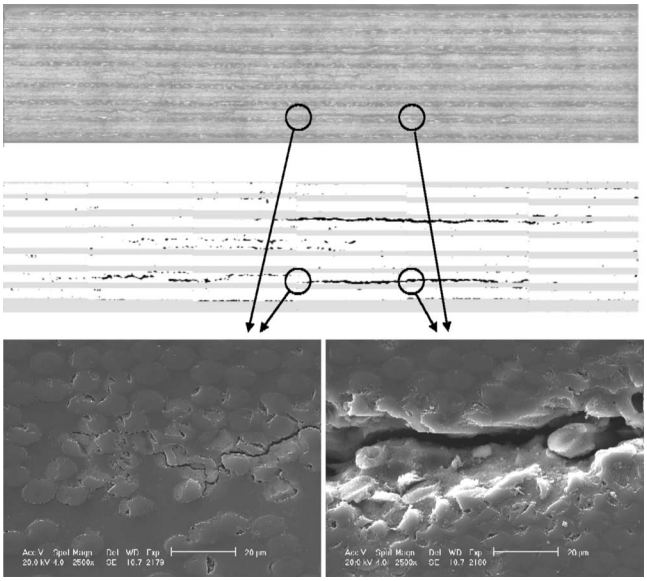

FIG. 7. Comparison between the original raw image and the post-treatment picture for crack detection. Details of the crack near its tip and its center.

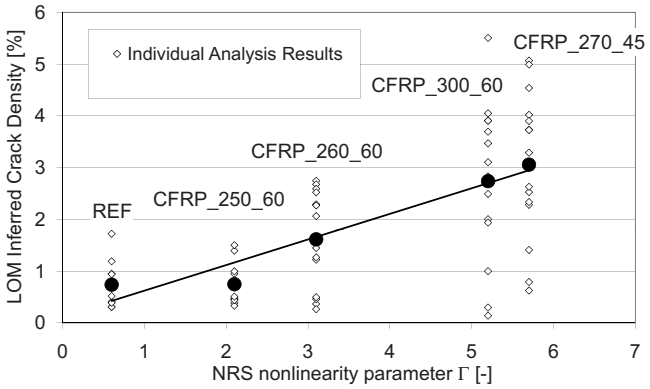

FIG. 8. Crack density versus NRS nonlinearity parameter Γ. Open diamonds are values of the crack density obtained for different parts of the images. Filled circles are the averages for the whole surface for each sample. The line is the linear trend line for the average values. The horizontal error bars for the experimentally obtained quantity of Γ are of a few percent for an individual sample.

(i) The NRS nonlinearity parameter increases with increasing crack density
(ii) The dispersion of the data increases with the NRS nonlinearity parameter. This can be explained by the non-homogeneous repartition of the cracks inside the samples.
(iii) Even though the crack density measurements for the reference sample and the sample treated at 250 °C for 60 min are not significantly different, the authors have observed a vast increase (more than a factor of 2) in the NRS nonlinearity parameter. This could imply that the authors' crack density procedure based on the image treatment is not sensitive enough to identify the very early features (e.g., increase in dislocation nuclei) that are responsible for the increased NRS nonlinearity parameter, even though they definitely exist. It again illustrates the extreme sensitivity of nonlinear techniques to early stages of damage.

V. NONLINEAR HYSTERETIC MODEL

The particular amplitude-dependent behavior of the resonance frequency after removing the external excitation can be modeled by a nonlinear extension of the Euler beam problem for flexural modes. Following the linear Euler beam theory, the true resonance frequency will be constant in the non-driven phase of reverberation. The nonlinear equation of motion in a one-dimensional flexural system, accounting for attenuation by introducing N relaxation mechanisms as was done by Blanch *et al.*,[35] reads

$$\frac{\partial v}{\partial t} = -\frac{1}{\rho}\frac{\partial \tau}{\partial x},$$

$$\frac{\partial \tau}{\partial t} = E(\tau, \dot{\tau}, \ldots)(1 + N\zeta)\left[\kappa^2 \frac{\partial^3 v}{\partial x^3} - \sum_{j=1}^{N} r_j\right] \tag{5}$$

with

$$\frac{\partial r_j}{\partial t} = -\frac{1}{\zeta_j} r_j + \frac{\zeta}{\zeta_j(1 + N\zeta)} \kappa^2 \frac{\partial^3 v}{\partial x^3},$$

$$\zeta = \frac{1}{Q_0} \frac{\int_{\omega_a}^{\omega_b} F(\omega;\zeta_1,\ldots,\zeta_N)d\omega}{\int_{\omega_a}^{\omega_b} [F(\omega;\zeta_1,\ldots,\zeta_N)]^2 d\omega},$$

and

$$F(\omega;\zeta_1,\ldots,\zeta_N) = \sum_{j=1}^{N} \frac{\omega\zeta_j}{1+\omega^2\zeta_j^2}.$$

The relaxation times ζ_j $(1 \leq j \leq N)$ and the number of mechanisms to be taken into account can be optimized to simulate a medium with constant Q_0 (quality factor) over a large frequency range $[\omega_a, \omega_b]$.[35]

In Eq. (5), v and τ are the particle velocity and the internal shear stress of the beam as functions of position x $(0 \leq x \leq L)$ and time t, E is the stress- and stress-rate-dependent Young's modulus, ρ is the mass density, and κ is the radius of gyration. In the case of the first fundamental mode, Eq. (3) provides the relation between the maximum amplitude of the internal shear strain η in the center of the beam and the maximum particle velocity v at the edges of the beam.[31,32]

In general, nonlinearity can be included by allowing the Young's modulus to depend on the shear stresses and shear stress rates [and if necessary other history-dependent variables, i.e., $E(\tau, \dot{\tau}, \ldots)$]. History and shear rate dependence of elastic moduli is typical of hysteretic media and has important consequences for the bookkeeping of the stress-strain or modulus-stress response when seeking a numerical solution since the value of the modulus needs to be updated at each time step and at each location based on (parts of) the previous shear stress history. Probably the most general method to deal with history-dependent moduli and hysteretic stress-strain relations is the Preisach–Mayergoysz (PM) approach. This technique follows the evolution of a statistical distribution of bistable elements as function of a control parameter (e.g., the shear stress) and transforms it into the evolution of the response function (e.g., the shear strain).[36–39] In the following simulations, the authors use the PM approach to take account of the nonlinearity.

Upon performing the numerical simulations, the geometrical parameters were measured for each sample, yielding input values for ρ and κ. Five relaxation mechanisms are assumed to provide a constant Q_0 value over a broad frequency range (0.1–5000 Hz). Further, the linear value of the Young's modulus E_0 and the linear quality factor Q_0 are adjusted to obtain the correct low amplitude values for each sample. They are assumed to be uniform over the beam length. The nonlinearity is introduced by specifying the statistical distribution of the bistable PM elements. The simplest way, which is most commonly used for dynamic processes, is to assume a uniform distribution of the elements. In this case, only one parameter is needed. The authors call γ the PM background density parameter [which is expressed in units of $(\text{Pa})^{-2}$][36–39] and assume that its value is uniform over the length of the sample (simulating a uniform distribution of damage). The physical meaning of the dimensionless quantity $\gamma dP_c dP_o$ is that it represents the deformation contribution of the hysteretic elements in the PM space with opening pressures between P_o and P_o+dP_o and closing pressures between P_c and P_c+dP_c upon switching from one state to the other (open to closed or closed to open). The larger γ, the larger the nonlinear strain contribution. This is the only free parameter to be used for fitting the nonlinear behavior.

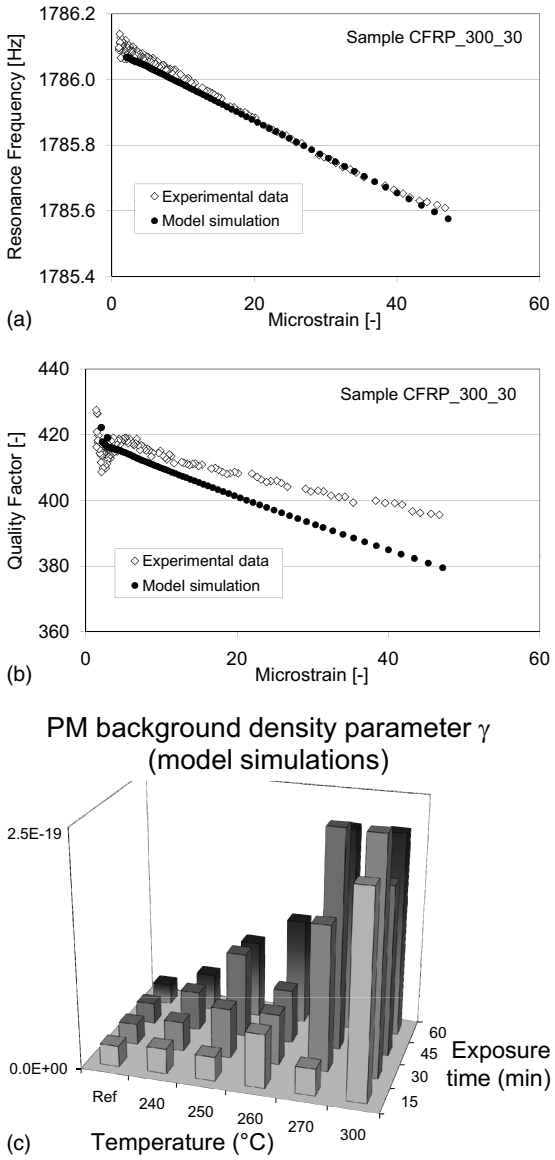

FIG. 9. Model results for CFRP_300_30 and comparison with experimental data. PM background density parameter γ used in the model simulations for all samples. The reference point was duplicated for different exposure times to help visualize the trend of the evolution of the parameters with temperature.

The numerical experiment is performed in the same way as the actual experiment. A harmonic forcing is applied for times $t < t_0$ and removed at t_0 [an external force can be added to the first equation in Eq. (5)]. The response in terms of particle velocity is calculated for $t < t_1$, with $t_0 < t_1$. Given the reverberation signal for $t_0 < t < t_1$, the authors apply the same analysis procedure, as was done for the experimental data, and fine-tune the values of E_0, Q_0, and γ so that the best agreement between model and experiment is obtained.

The comparison of the results for an exposure to 300 °C for 30 min is shown in Fig. 9. The simulations track the experimentally observed resonance frequency reduction extremely well. For the nonlinearity in the damping, the experi-

mental data are generally noisier. Nevertheless, the authors find more or less the same tendency as that predicted in the simulations (with a 5% error at 50 microstrain). The discrepancy could be due to the non-ideal experimental support of the beams by the nylon wires located at the node lines.

Three important issues about the nonlinearity parameter quantification should be noted.

(1) The use of reversible nonlinear models, such as the polynomial expansion of stress versus strain (or vice-versa),[26] would lead to a quadratic behavior of the resonance frequency shift with amplitude and does not affect the attenuation characteristic. To find the linear decrease observed in the data for the resonance frequency and the quality factor Q, it is essential to start from a hysteretic model.
(2) The PM background density parameter γ used in the numerical model is quite small. For the simulation of the nonlinear effects measured in the experiments, the authors used a value of γ between 2.2×10^{-20} Pa^{-2} (reference sample) and 2.2×10^{-19} Pa^{-2} (300 °C for 60 min). As mentioned above, $\gamma dP_c dP_o$ represents the deformation contribution of the hysteretic elements in the PM space with opening pressures between P_o and P_o+dP_o and closing pressures between P_c and P_c+dP_c upon switching from one state to the other. If the authors assumed a constant density in the statistical PM space, ranging from -5 to 5 MPa, this would amount to a total hysteretic contribution to the strain of only $\gamma\int_{-5\ \mathrm{MPa}}^{5\ \mathrm{MPa}}\int_{-5\ \mathrm{MPa}}^{P_0} 1 dP_c dP_0 = \gamma\frac{1}{2}10^{14} \approx 10^{-6}-10^{-5}$ when changing the stress from -5 to 5 MPa.
(3) Based on the PM space approach,[36–39] the relative modulus change is—at first order of approximation—proportional to the constant background density parameter γ of the PM space, the linear modulus E_0, and the stress change itself. Since stress and strain are linked by the modulus, the authors obtain $[E_0-E(\eta)]/E_0 \propto \gamma E_0^2 \eta$.

For those levels of nonlinear behavior observed in this study, giving rise to small frequency or modulus shifts, the authors indeed obtain in all cases a constant ratio between the macroscopically observed NRS nonlinearity parameter Γ and the theoretically found microscopic nonlinearity, which is expressed by the PM background density parameter γ: $(\Gamma/\gamma)(12/E_0)^2=1$.

VI. CONCLUSION

In this paper, the authors demonstrated the efficiency of the NRS technique to detect damage. NRS is the time domain analog of the SIMONRUS technique. Examples for global damage features in the case of thermal exposure on CFRP beams were given. The authors applied a crack density imaging procedure and managed to obtain the first ever quantification of the nonlinearity signature in terms of the crack density. This result confirms that the increase in nonlinearity is linked to an increased network of cracks and that the nonlinear signature is even sensitive to microscopic alterations (e.g., dislocations) in the microstructure well before the visualization threshold for microcracks by the currently used optical technique. Numerical simulations of wave resonances based on a uniform distribution of a hysteretic nonlinear constitutive relation within the sample support the results and relate the macroscopic NRS nonlinearity parameter to the microscopic PM background density parameter of hysteretic (bistable) elements.

The NRS technique has the advantage to be fast; it has low or no restrictions on the sample geometry; and in most cases it can be implemented in a fully non-contact manner (due to the low frequency nature of the method). On the other hand, it necessitates free (or at least steady, amplitude-independent) boundary condition and is only applicable for low attenuation materials.

ACKNOWLEDGMENTS

The authors gratefully acknowledge the support of the European FP6 Grant AERONEWS (Grant No. AST-CT-2003-502927), the Flemish Fund for Scientific Research (Grant Nos. G.0206.02, G.0554.06, and G.0443.07), the Research Council of the Katholieke Universiteit Leuven (Grant Nos. OT/07/051 and CIF1), and the institutional support of the Los Alamos National Laboratory.

[1] P. A. Johnson, "The new wave in acoustic testing," Mater. World **7**, 544–546 (1999).
[2] P. P. Delsanto, *The Universality of Nonclassical Nonlinearity with Applications to NDE and Ultrasonics* (Springer, New York, 2006).
[3] O. Buck, W. L. Morris, and J. M. Richardson, "Acoustic harmonic-generation at unbonded interfaces and fatigue cracks," Appl. Phys. Lett. **33**, 371–373 (1978).
[4] J. H. Cantrell and W. T. Yost, "Acoustic harmonic-generation from fatigue-induced dislocation dipoles," Philos. Mag. A **69**, 315–326 (1994).
[5] P. B. Nagy and L. Adler, "Acoustic nonlinearity in plastics," in *Review of Progress in Quantitative Nondestructive Evaluation*, edited by D. O. Thompson and D. E. Chimenti (Plenum, New York, 1992), Vol. **11B**, pp. 2025–2032.
[6] K. Van Den Abeele, A. Sutin, and P. A. Johnson, "Nonlinear elastic wave spectroscopy (NEWS) techniques to discern material damage. Part I: Nonlinear wave modulation spectroscopy (NWMS)," Res. Nondestruct. Eval. **12**, 17–30 (2000).
[7] V. V. Kazakov, A. Sutin, and P. A. Johnson, "Sensitive imaging of an elastic nonlinear wave-scattering source in a solid," Appl. Phys. Lett. **81**, 646–648 (2002).
[8] A. Zagrai, D. Donskoy, A. Chudnovsky, and E. Golovin, "Micro- and macroscale damage detection using the nonlinear acoustic vibro-modulation technique," Res. Nondestruct. Eval. **19**, 104–128 (2008).
[9] C. R. P. Courtney, B. W. Drinkwater, S. A. Neild, and P. D. Wilcox, "Factors affecting the ultrasonic intermodulation crack detection technique using bispectral analysis," NDT & E Int. **41**, 223–234 (2008).
[10] T. J. Ulrich, P. A. Johnson, and R. A. Guyer, "Interaction dynamics of elastic waves with a complex nonlinear scatterer through the use of a time reversal mirror," Phys. Rev. Lett. **98**, 104301 (2007).
[11] V. Nazarov, L. Ostrovsky, I. Soustova, and A. Sutin, "Nonlinear acoustics of micro-inhomogeneous media," Phys. Earth Planet Inter. **50**, 65–73 (1988).
[12] P. A. Johnson, B. Zinszner, and P. N. J. Rasolofosaon, "Resonance and elastic nonlinear phenomena in rock," J. Geophys. Res. **101**, 11553–11564 (1996).
[13] K. Van Den Abeele, J. Carmeliet, J. A. TenCate, and P. A. Johnson, "Nonlinear elastic wave spectroscopy (NEWS) techniques to discern material damage. Part II: Single-mode nonlinear resonance acoustic spectroscopy," Res. Nondestruct. Eval. **12**, 31–42 (2000).
[14] P. A. Johnson, B. Zinszner, P. Rasolofosaon, K. Van Den Abeele, and F. Cohen-Tenoudji, "Dynamic measurements of the nonlinear elastic parameter alpha in rock under varying conditions," J. Geophys. Res. **109**, 10129–10139 (2004).
[15] P. A. Johnson and A. Sutin, "Slow dynamics and anomalous nonlinear fast dynamics in diverse solids," J. Acoust. Soc. Am. **117**, 124–130 (2005).

[16]J. A. TenCate and T. J. Shankland, "Slow dynamics in the nonlinear elastic response of Berea sandstone," Geophys. Res. Lett. **23**, 3019–3022 (1996).
[17]J. A. TenCate, E. A. Smith, and R. A. Guyer, "Universal slow dynamics in granular solids," Phys. Rev. Lett. **85**, 1020–1023 (2000).
[18]M. Bentahar, H. El Aqra, R. El Guerjouma, M. Griffa, and M. Scalerandi, "Hysteretic elasticity in damaged concrete: Quantitative analysis of slow and fast dynamics," Phys. Rev. B **73**, 014116 (2006).
[19]M. Vila, F. Vander Meulen, S. Dos Santos, L. Haumesser, and O. Bou Matar, "Contact phase modulation method for acoustic nonlinear parameter measurement in solid," Ultrasonics **42**, 1061–1065 (2004).
[20]P. B. Nagy, "Fatigue damage assessment by nonlinear ultrasonic materials characterization," Ultrasonics **36**, 375–381 (1998).
[21]K. Van Den Abeele, K. Van De Velde, and J. Carmeliet, "Inferring the degradation of pultruded composites from dynamic nonlinear resonance measurements," Polym. Compos. **22**, 555–567 (2001).
[22]K. Van Den Abeele and J. De Visscher, "Damage assessment in reinforced concrete using spectral and temporal nonlinear vibration technique," Cem. Concr. Res. **30**, 1453–1464 (2000).
[23]C. Payan, V. Garnier, J. Moysan, and P. A. Johnson, "Applying nonlinear resonant ultrasound spectroscopy to improving thermal damage assessment in concrete," J. Acoust. Soc. Am. **121**, EL125–EL130 (2007).
[24]K. Van Den Abeele, C. Campos-Pozuelo, J. Gallego-Juarez, F. Windels, and B. Bollen, "Analysis of the nonlinear reverberation of titanium alloys fatigued at high amplitude ultrasonic vibration," in Proceedings Forum Acustica Sevilla 2002, (2002).
[25]R. A. Guyer and P. A. Johnson, "Nonlinear mesoscopic elasticity: Evidence for a new class of materials," Phys. Today **52**, 30–36 (1999).
[26]R. A. Guyer, K. R. McCall, and K. E. A. Van Den Abeele, "Slow elastic dynamics in a resonant bar of rock," Geophys. Res. Lett. **25**, 1585–1588 (1998).
[27]R. P. Taylor, "Fiber composite aircraft-capability and safety," Australian Transport Safety Bureau Report No. AR-2007-021, 2008, p. 6, available at http://www.atsb.gov.au/media/27758/ar2007021.pdf (Last viewed July 27, 2009); P. Trum, "Living in a composite material world," in Headway, Research Discovery and Innovation at McGill University, available at http://www.mcgill.ca/headway/winter2008-09/industrialimpact1/ (Last viewed July 27, 2009); "Composite materials and aircraft structures certificate programs overview," University of Washington, College of Engineering, available at http://www.engr.washington.edu/epp/cmc/ (Last viewed July 27, 2009).
[28]G. A. Matzkanin and G. P. Hansen, "Heat damage in graphite epoxy composites: Degradation, measurement and detection—A state-of-the-art report," Report No. NTIAC-SR-98-02, NTIAC, 1998.
[29]G. A. Matzkanin, "Nondestructive characterization of heat damage in graphite/epoxy composite: A state-of-the-art report," Texas Research Institute, Austin, TX, 1995.
[30]F. Hyllengren, Technical Report No. TEK01-0022, C. S. M. Materialteknik, Linköping, Sweden, 2001.
[31]M. Geradin and D. Rixen, *Mechanical Vibrations: Theory and Application to Structural Dynamics* (Wiley, Chichester, 1994).
[32]J. W. Strutt and B. Rayleigh, *The Theory of Sound* (Mac Millan, New York, 1894), Vol. **1**, Chap. 8.
[33]GIMP, GNU Image Manipulation Program, User Manual, Edge-Detect Filters, Sobel, The GIMP Documentation Team, 2008.
[34]T. Acharya and A. K. Ray, *Image Processing: Principles and Applications* (Wiley-Interscience, New York, 2005), pp. 111–113.
[35]J. O. Blanch, J. O. A. Robertsson, and W. W. Symes, "Modeling of a constant-Q-methodology and algorithm for an efficient and optimally inexpensive viscoelastic technique," Geophysics **60**, 176–184 (1995).
[36]K. R. McCall and R. A. Guyer, "Equation of state and wave propagation in hysteretic nonlinear elastic materials," J. Geophys. Res. **99**, 23887–23897 (1994).
[37]R. A. Guyer, K. R. McCall, and G. N. Boittnott, "Hysteresis, discrete memory, and nonlinear-wave propagation in rock—A new paradigm," Phys. Rev. Lett. **74**, 3491–3494 (1995).
[38]K. Van Den Abeele, F. Schubert, V. Aleshin, F. Windels, and J. Carmeliet, "Resonant bar simulations in media with localized damage," Ultrasonics **42**, 1017–1024 (2004).
[39]K. Van Den Abeele and S. Vanaverbeke, "Multiscale approach and simulations of wave propagation and resonance in media with localized microdamage: 1D and 2D cases," in *The Universality of Nonclassical Nonlinearity with Applications to NDE and Ultrasonics*, edited by P. P. Delsanto (Springer, New York, 2006), Chap. 12, pp. 177–202.